Object representation and distance encoding in three-dimensional environments by a neural circuit in the visual system of the blowfly

Pei Liang, Jochen Heitwerth, Roland Kern, Rafael Kurtz and Martin Egelhaaf

J Neurophysiol 107:3446-3457, 2012. First published 14 March 2012; doi:10.1152/jn.00530.2011

J Neurophysiol 107: 3446–3457, 2012.
First published March 14, 2012; doi:10.1152/jn.00530.2011.

Object representation and distance encoding in three-dimensional environments by a neural circuit in the visual system of the blowfly

Pei Liang, Jochen Heitwerth, Roland Kern, Rafael Kurtz, and Martin Egelhaaf
Neurobiology and Cognitive Interaction Technology Center of Excellence (CITEC), Bielefeld University, Bielefeld, Germany

Submitted 13 June 2011; accepted in final form 12 March 2012

Liang P, Heitwerth J, Kern R, Kurtz R, Egelhaaf M. Object representation and distance encoding in three-dimensional environments by a neural circuit in the visual system of the blowfly. *J Neurophysiol* 107: 3446–3457, 2012. First published March 14, 2012; doi:10.1152/jn.00530.2011.—Three motion-sensitive key elements of a neural circuit, presumably involved in processing object and distance information, were analyzed with optic flow sequences as experienced by blowflies in a three-dimensional environment. This optic flow is largely shaped by the blowfly's saccadic flight and gaze strategy, which separates translational flight segments from fast saccadic rotations. By modifying this naturalistic optic flow, all three analyzed neurons could be shown to respond during the intersaccadic intervals not only to nearby objects but also to changes in the distance to background structures. In the presence of strong background motion, the three types of neuron differ in their sensitivity for object motion. Object-induced response increments are largest in FD1, a neuron long known to respond better to moving objects than to spatially extended motion patterns, but weakest in VCH, a neuron that integrates wide-field motion from both eyes and, by inhibiting the FD1 cell, is responsible for its object preference. Small but significant object-induced response increments are present in HS cells, which serve both as a major input neuron of VCH and as output neurons of the visual system. In both HS and FD1, intersaccadic background responses decrease with increasing distance to the animal, although much more prominently in FD1. This strong dependence of FD1 on background distance is concluded to be the consequence of the activity of VCH that dramatically increases its activity and, thus, its inhibitory strength with increasing distance.

optic flow; visual motion

INFORMATION ABOUT OBJECTS and the spatial layout of the environment is highly relevant for animals moving in cluttered environments, in particular when required to avoid obstacles or, in the case of flying animals, to prepare for landing. An object can be discriminated from its background on the basis of different texture properties such as color, shape, contrast, and luminance. Even if all these features are shared by the background, an object can be detected by a moving observer just from the relative motion between the object and its more distant background. Thus object detection is possible even without stereoscopic vision. Object detection based on motion cues is particularly relevant for rapidly moving animals, because they have to make behavioral decisions, such as initiating collision avoidance, at some distance to these objects. The optic flow, i.e., the continuous displacements of the animals' retinal images during self-motion, provides depths cues especially during rapid motion and can be used to segregate objects from background structures (Koenderink 1986). Indeed, many animals, including humans, have been shown to strongly rely on optic flow for spatial vision and object detection (review in Kral 2003; humans: Lappe et al. 1999; Regan and Beverly 1984; Warren et al. 2001; monkeys: Miles 1998; pigeons: Frost and Nakayama 1983; Wylie and Frost 1999; insects: Egelhaaf 1985a; Kimmerle et al. 1996; Reichardt et al. 1983; Srinivasan et al. 1990; Virsik and Reichardt 1976).

However, the ability to gain spatial information from optic flow and to detect objects by relative motion cues is limited to translational self-motion. In contrast, rotations lead to retinal velocities that are independent from the distance to objects. Most realistic optic flow fields can be decomposed mathematically into their rotational and translational components (Dahmen et al. 2000; Longuet-Higgins and Prazdny 1980; Prazdny 1980). Nonetheless, several insect groups, such as flies (Braun et al. 2010; Geurten et al. 2010; Schilstra and van Hateren 1999; van Hateren and Schilstra 1999), flying hymenopterans (Boeddeker et al. 2010; Braun et al. 2012), and orthopterans (Kral 2009), but also birds such as zebra finches (Eckmeier et al. 2008), employ another strategy to reduce the complexity of the optic flow. By pursuing a smart active gaze strategy, they separate the translational optic flow components from the rotational ones: They shift their gaze by brief saccadic rotations of body and head that last less than 20% of the entire flight time, keeping their gaze virtually constant during translational locomotion between saccades (intersaccadic intervals), which thus correspond to more than 80% of the flight time (Boeddeker et al. 2010; Braun et al. 2010, 2012; Geurten et al. 2010; Schilstra and van Hateren 1999; van Hateren and Schilstra 1999).

How does the neural representation of the optic flow induced by intersaccadic translational self-motion reflect information about the three-dimensional layout of the environment? So far, this is largely unknown for most animals, since stimuli not suited to answer this question, such as constant velocity stimuli or white-noise velocity fluctuations, have been used for analysis of motion-sensitive neurons in most studies. Exceptions are studies in which the optic flow generated on movement trajectories in three-dimensional virtual environments has been employed to characterize motion-sensitive neurons, for instance, in area MST of macaques (e.g., Logan and Duffy 2005). However, only in flies have motion-sensitive visual neurons been recorded during stimulation with behaviorally generated stimuli, which emulate the characteristic dynamic conditions encountered by freely flying animals (Boeddeker et al. 2005; Karmeier et al. 2006; Kern et al. 2005, 2006; van Hateren et al. 2005). The fly is an excellent animal model in which to study visual information processing, because neurons involved in optic flow processing are relatively easy to access

Address for reprint requests and other correspondence: M. Egelhaaf, Neurobiology and CITEC, Bielefeld Univ., Universitätsstr. 25, D-33615 Bielefeld, Germany (e-mail: martin.egelhaaf@uni-bielefeld.de).

experimentally, and it is possible to associate neuronal response properties with their significance for behavior (reviews in Borst and Haag 2002, 2010; Egelhaaf 2006, 2009; Egelhaaf et al. 2002). These neurons reside in the fly's third visual neuropil, the lobula plate, and are termed lobula plate tangential cells (LPTCs) (Borst and Haag 2002, 2010; Egelhaaf 2006, 2009; Egelhaaf et al. 2002; Hausen 1981, 1984; Krapp 2000). Most of them have extended dendrites on which they spatially integrate the outputs of retinotopically arranged local motion-sensitive elements. As a consequence of this input, LPTCs respond in a direction-selective way to motion in large parts of the visual field. However, LPTCs may also receive input from other LPTCs and, thus, form an intricate neural network that processes optic flow information.

An identified neural circuit built of several types of LPTCs is thought to be involved in object detection (Fig. 1). The figure-detection (FD) cells (Egelhaaf 1985b) are the output elements of the circuit and possess, similar to many other LPTCs, a large excitatory receptive field. They do not respond most strongly when a motion stimulus extends across the entire receptive field, but when a moving object of limited size is presented. This small-field tuning of FD cells has been suggested to be accomplished by processing of local excitatory inputs with additional inhibitory input (Egelhaaf 1985c; Hennig et al. 2008). The inhibitory input is supplied by another LPTC, the GABAergic ventral centrifugal horizontal (VCH) neuron (Warzecha et al. 1993), which provides information on large-field motion in the ipsi- and contralateral visual field (Eckert and Dvorak 1983; Egelhaaf et al. 1993; Gauck et al. 1997; Hausen 1976; Hennig et al. 2011). VCH receives relatively strong excitatory contralateral synaptic input from two neurons, H1 and H2, both of which are excited by back-to-front motion and inhibited by front-to-back motion (Eckert and Dvorak 1983; Egelhaaf et al. 1993; Gauck et al. 1997; Haag and Borst 2001; Hausen 1981; Hennig et al. 2011; Krapp et al. 2001; van Hateren et al. 2005). Moreover, VCH receives inhibitory input from Hu, a cell that is excited by front-to-back motion in the contralateral visual field of VCH and inhibited by motion in the reverse direction. Further key elements of the circuit, the horizontal system (HS) cells, provide the major ipsilateral input to the VCH cell, to which they are coupled via dendrodendritic electrical synapses. In addition, HS neurons are major output neurons of the optic lobes (Haag and Borst 2002; Hennig et al. 2011). HS cells are involved in processing optic flow during locomotion in the horizontal plane. They are maximally excited during global horizontal motion, which is induced during turns of the fly around its vertical body axis (Hausen 1982a, 1982b; Horstmann et al. 2000; Krapp et al. 2001), or translation, which is characteristic of the intersaccadic interval (Karmeier et al. 2006; Kern et al. 2005). The intersaccadic responses of HS cells have been shown to depend on the spatial layout of the environment (Boeddeker et al. 2005; Karmeier et al. 2006; Kern et al. 2005, 2006). Moreover, they are excited when an object suddenly moves in the preferred direction into their receptive fields (Liang et al. 2008, 2011; O'Carroll et al. 2011). Thus both FD and HS cells are likely to play an essential role in providing spatial information for guiding orientation behavior.

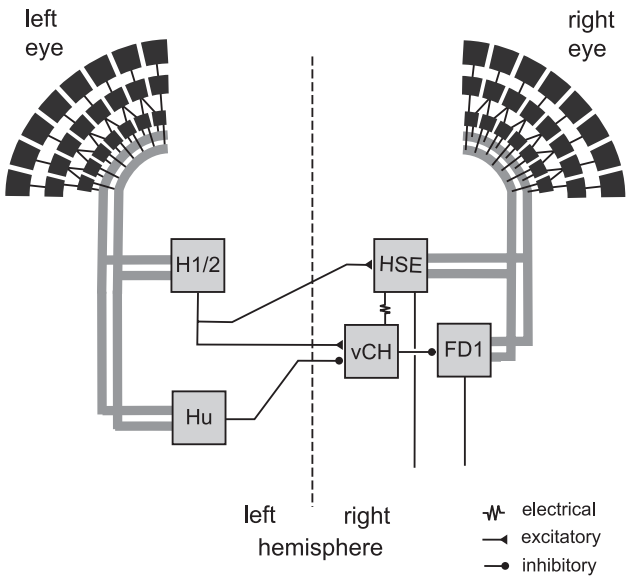

Fig. 1. Schematic diagram of part of the neural circuit that provides the fly with information about objects and spatial properties of its environment. The right figure-detection (FD1) cell and its input elements relevant to this study are shown [for sake of clarity, of the 3 horizontal system (HS) cells, only HSE is shown]. All neurons have a horizontal preferred direction. FD1 and the HS cells receive retinotopic motion input (thick gray lines) from large parts of the ipsilateral eye. The right ventral centrifugal horizontal (VCH) cell is electrically coupled with the right HSE and HSS cells and inhibits the right FD1 cell. The left H1 and the left H2 excite the right VCH, HSE, and HSN. In addition, the left Hu cell inhibits the right VCH. FD1 and HS cells are output neurons of the optic lobe, whereas H1, H2, Hu, and VCH connect exclusively to other lobula plate tangential cells (LPTCs).

In the present study, we have addressed the issue of how spatial information is represented during intersaccadic intervals by the key elements of the sketched neural circuit. We employed two different stimulation paradigms that address different issues. *1*) To address the efficiency with which these neurons represent object information, the responses to optic flow as experienced during semi-free flight in a flight arena were compared between one type of FD cell (FD1), the VCH cell, and HS cells (HSS, HSE, HSN). The behaviorally generated optic flow was modified by inserting objects close to the flight trajectory (Fig. 2). *2*) To address to what extent the distance to extended background structures is encoded, we analyzed the responses of HS cells to stimuli reconstructed from semi-free-flight trajectories. To this end, the original flight arena was virtually modified by systematically changing its size and thus its overall distance to the fly.

MATERIALS AND METHODS

Visual Stimulation

Two visual stimulation paradigms were employed in the object representation and in the distance encoding experiments. A free-flight trajectory of a blowfly (*Calliphora vicina*) monitored in a flight arena with textured walls (Schilstra and van Hateren 1999; van Hateren and Schilstra 1999) formed the basis of the object representation experiments. The optic flow generated on the eyes of the fly while flying this trajectory in the original and in an enlarged arena, both with and without two inserted cylindrical objects, was then used for stimulation in the electrophysiological analysis. The distance encoding experiments were based on three different trajectories from three different flies placed in various differently sized arenas (for details see methods in Lindemann et al. 2003).

Generation of visual stimuli for object representation experiments. A flight trajectory (duration 3.45 s) was chosen from a large data set

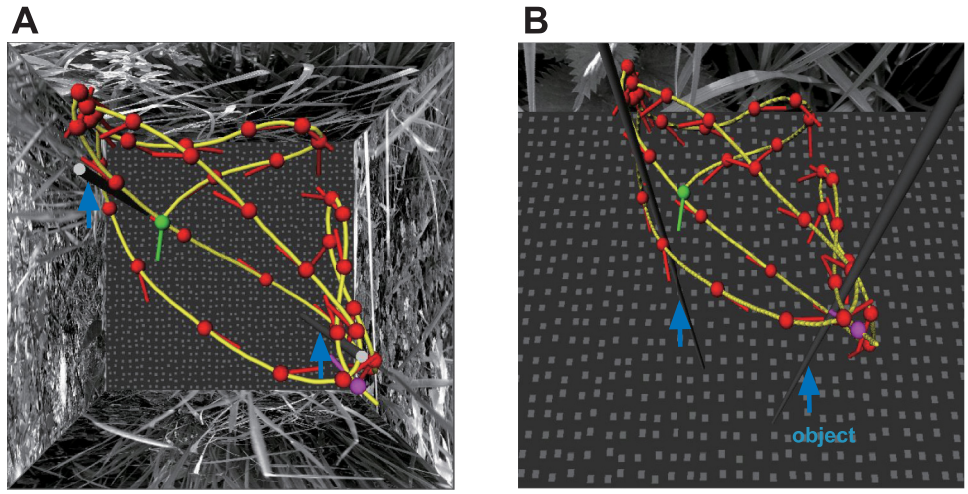

Fig. 2. Flight trajectory of a blowfly in a cubic arena used for the reconstruction of optic flow. The track of the fly is indicated by the yellow lines; red dots and short dashes indicate the position of the fly's head and its orientation, respectively; green and violet dots indicate the start and end of the trajectory, respectively. *A*: top view of the complete trajectory in the small arena (edge length 0.4 m). *B*: top view of same trajectory in the large arena (edge length 2.0 m). In some of the stimulus sequences, 2 virtual objects (homogeneous black cylinders, diameter 10 mm, marked by blue arrows) were inserted at positions very close to the trajectory.

provided by Dr. J. H. van Hateren (University of Groningen, Groningen, The Netherlands). The data were obtained from blowflies flying in a cubic arena (edge length 0.4 m; walls covered with photographs of herbage, Fig. 2). The root mean square contrast of this pattern was ~0.6. However, the contrast fluctuated considerably when determined within spatial windows in the range of the analyzed cell's receptive field size (for details, see Liang et al. 2011). The arena was placed in a Helmholtz coil; the position and orientation of the blowfly's head were monitored by measuring the voltage induced in miniature sensor coils, which were mounted on it (van Hateren and Schilstra 1999). The semi-free-flight sequences recorded in this way do not differ in their saccadic structure from free-flight maneuvers monitored with high-speed cameras (Boeddeker et al. 2005). With known gaze direction and visual interior of the cage, the visual stimuli could be reconstructed and presented in a panoramic LED display instrument, called FliMax (Lindemann et al. 2003). To introduce spatial discontinuities, two homogenous black vertical cylinders (diameter 0.01 m, height 0.4 m) were virtually inserted into the flight arena close to the flight trajectory (which was recorded without objects). The corresponding modified image sequence was reconstructed using methods similar to those in our previous studies (Liang et al. 2008, 2011). To modify spatial discontinuities, the size of the flight arena was changed virtually, i.e., its edge length was increased to 2 m (large arena). The wall pattern and the height of the objects were scaled accordingly, but the distance between objects and fly remained unchanged. To remove the influence of background motion, we changed the wall pattern of the arena to homogeneous gray while the positions of objects remained unchanged. Altogether, the conditions described above add up to five different stimuli (O-nB: object, no background; nO-cB: no object, close background; O-cB: object, close background; nO-dB: no object, distant background; O-dB: object, distant background; see RESULTS for details), which were presented in pseudorandom order. Between two stimuli, all LEDs of FliMax were set to the mean luminance of the previously presented stimulus for 20 s to allow the fly's visual system to return to the same adaptation level before each stimulus run.

Generation of visual stimuli for distance encoding experiments. Three flight trajectories from three different flies, each lasting 3.45 s, were chosen from a large data set obtained from blowflies flying in a cubic arena (the same as that described for object representation experiments). To analyze how the membrane potential of HSE encodes the distance between the fly and the arena walls, we recorded its responses to the three original flight trajectories in the original arena (edge length 0.4 m). Because distance could not exceed 0.55 m (diagonal of the original arena) when the original arena was used, we performed additional experiments in which we set the edge length of the cubic arena to 0.41, 0.55, 1.05, 2.35, and 7.35 m. Here, the otherwise unaltered flight trajectory was centered in the virtual arena before rendering, resulting in minimum distances of the trajectory from the arena walls of 30, 100, 350, 1,000, and 3,500 mm, respectively. Although only the HSE cell in the right brain hemisphere was recorded in these experiments, we obtained an approximation of the responses of the HSE in the left brain hemisphere during the same flight by presenting a flipped version of the reconstructed optic flow.

Electrophysiological Analysis

One- to three-day-old female blowflies (*C. vicina*) were dissected as described previously (Dürr and Egelhaaf 1999). Temperature during experiments, measured close to the animal, was 24–34°C. Voltage responses were recorded intracellularly with glass electrodes (GC100TF-10; Clark Electromedical Instruments, Pangbourne Reading, UK) from the axon of HS or VCH cells in the right brain hemisphere. These neurons respond with graded changes of their axonal membrane potential to visual motion. In the HS neurons, these graded changes are superimposed with spikes of variable amplitude. The resistance of the intracellular electrodes, filled with 1 M KCl, was 20–50 MΩ. Ringer solution (Kurtz et al. 2000) was used to prevent desiccation of the brain. Extracellular recordings of FD1 cells were done with glass electrodes (G100TF-4; Warner Instruments, Hamden, CT) that had resistances of 2–5 MΩ when filled with 1 M KCl. All electrodes were pulled on a P97 Puller (Sutter Instruments, Novato,

Fig. 3. Averaged time-dependent responses of 3 HSN, 3 VCH, and 5 FD1 cells to 5 different optic flow stimuli (see chart, *inset*). *A1*, *B1*, and *C1* show responses to the optic flow induced by the dark objects alone, with the background homogenously lit at half-maximum brightness of the stimulus arena (O-nB). *A2*, *B2*, and *C2* show responses to the motion sequence experienced by the fly in the small arena (close background) with (O-cB, red curves) and without objects (nO-cB, blue curves). *A3*, *B3*, and *C3* show responses with (O-dB) and without objects (nO-dB), similar to the motion sequence in *A2*, *B2*, and *C2*, but in the large arena (distant background). Green columns in all diagrams mark the time windows within intersaccadic intervals when objects appeared in the receptive field of FD1 cells as determined by the FD1 response shown in *C1*. Note that these time windows were shifted to account for the different response delays of the neurons (see MATERIALS AND METHODS). The object-induced response increments are visible in the responses of HSN and FD1 (compare red and blue curves in *A2–A3* and *C3–C4*, respectively). These increments are most pronounced for FD1 cells in the large arena (*C3*). The yaw velocity during the corresponding flight (see Fig. 2) is shown to the *left* of the chart *inset*. Enlarged sections of the traces shown in *A2*, *B2*, and *C2* are plotted in *A4*, *B4*, and *C4*; the corresponding yaw velocity section is shown to the *right* of the chart *inset*.

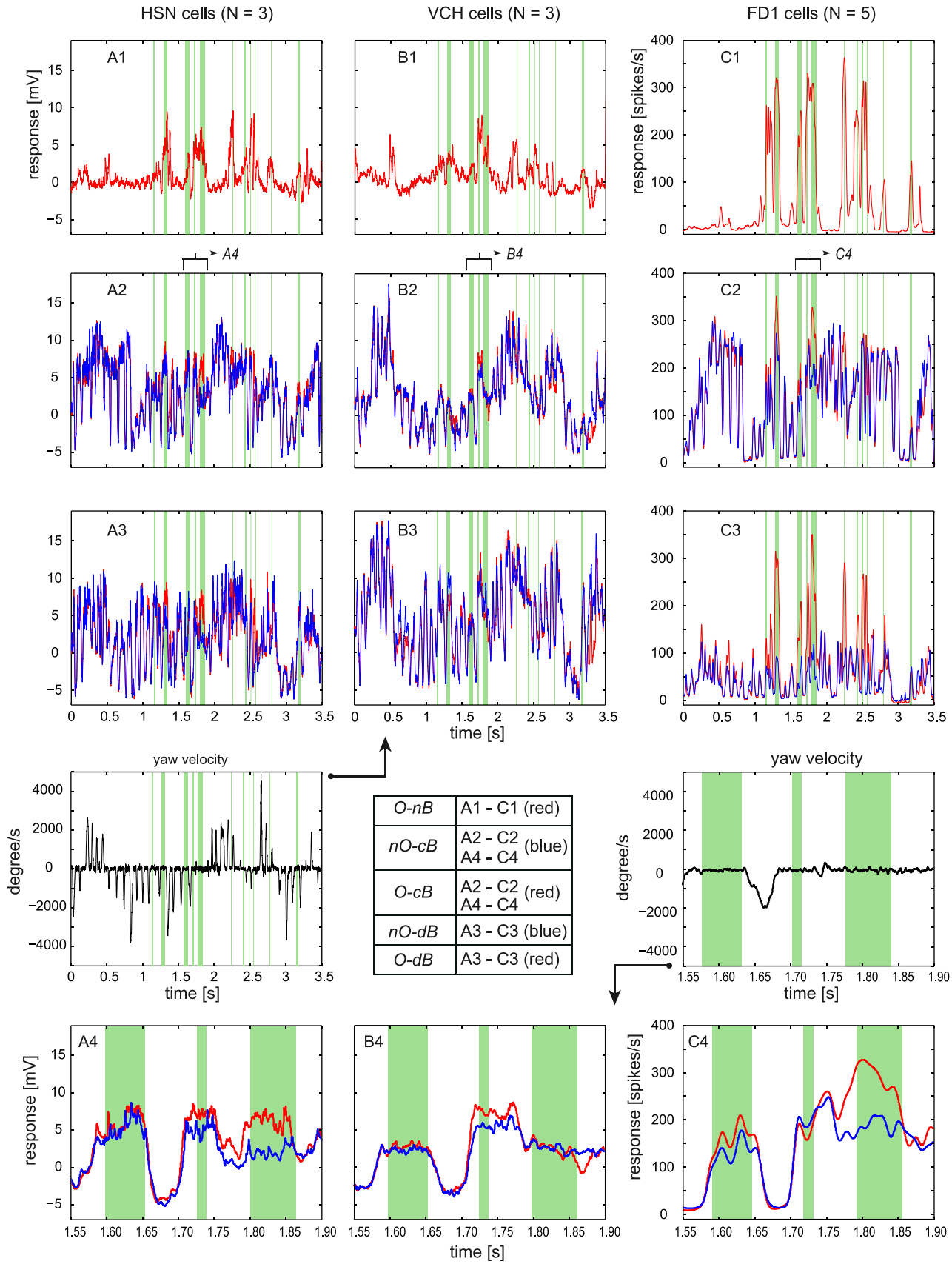

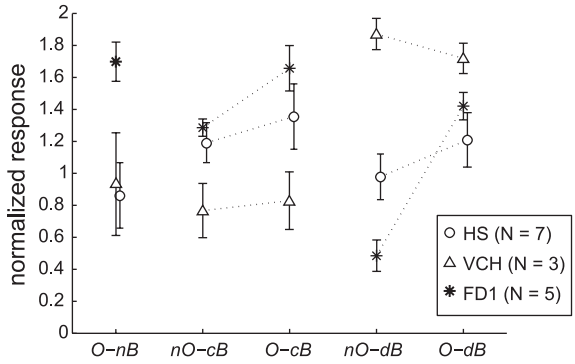

Fig. 4. Normalized object and background responses (±SD) of HS, VCH, and FD1 cells under 5 different stimulus conditions (*x*-axis) are averaged from the time windows marked in Fig. 3 (green). Dotted lines connect the responses in the same flight arena with and without objects. The responses were normalized by dividing, for each recorded cell, the half-wave rectified responses to the different stimulus conditions by the corresponding response obtained for the small arena without objects (nO-cB), time-averaged over the entire data trace. Normalization values for the individual cells of each cell type were as follows: FD1 (spikes/s): 120, 103, 157, 147, 147; HSS (mV): 6.9, 3.7; HSE (mV): 10.4, 3.8; HSN (mV): 5.1, 3.8, 2.8; VCH (mV): 3.6, 3.3, 2.7. Number of sweeps per cell type in the order of the plotted conditions (O-nB, nO-cB, O-cB, nO-dB, O-dB) was as follows: FD1: 66, 65, 63, 67, 65; HSS: 22, 21, 22, 21, 22; HSE: 10, 10, 10, 10, 11; HSN: 12, 13, 15, 11, 12; VCH: 13, 13, 17, 14, 16.

CA). Recording site was the input arborization of the FD1 cell in the right optic lobe. The amplified, bandpass-filtered (low pass, 10 kHz; high pass, 200 Hz) raw signals were sampled at 20 kHz (DT 3001; Data Translation, Marlboro, MA) and stored on hard disk for off-line analysis.

Analysis of Data Obtained in the Object Detection and Distance Encoding Experiments

The numbers of HS, FD1, and VCH cells recorded in the object detection experiments are specified in RESULTS. The number of HSE cells recorded in the distance encoding experiments was different for the various arena sizes and is specified in the legend of Fig. 6. Some of the latter data have already been used in Kern et al. (2005) for analyzing different aspects of optic flow processing. All data were analyzed with MATLAB 7.9 (The MathWorks, Natick, MA). The spike activities of FD1 cells were transformed into peristimulus time histograms (temporal resolution 4 ms). For FD1, we subtracted the baseline spike activity (averaged over 500 ms before stimulation) from the overall activity. For HS and VCH, we subtracted the resting potential (averaged over 500 ms before stimulation) from the intracellularly recorded membrane potential (Fig. 3). To facilitate comparison of the responses of the different types of cells (Fig. 4), we normalized for each individual cell all responses to the time-averaged responses in the small arena without object (condition: nO-cB). Before normalization, half-wave rectification was applied to all responses to eliminate the negative signal components introduced by subtracting the resting activity. Hence, only the response components resulting from motion in the particular cell's preferred direction were used for this part of the analysis.

To analyze the impact of an object on the cellular responses, we quantified the responses in those intersaccadic intervals where an object passes the particular cell's receptive field (object response). These responses were compared with the responses in the same intersaccadic intervals without objects (background response). The intersaccadic intervals were selected by masking saccades (see methods in Kern et al. 2005). Briefly, saccades were detected by peaks in angular head velocity (threshold 500°/s), and saccades that were close together were merged. To define the time windows when an object is present in the receptive field and moving in the preferred direction, we used the FD1 responses to the reference stimulus where the dark objects are shown against a nontextured, homogeneous gray background. Because the horizontal extent of the most sensitive part of the receptive field of FD1 cells largely overlaps those of HS and VCH cells, the same time windows could be used for all three cell types. The windows for time intervals in which object responses were evaluated had to satisfy two criteria: *1*) the averaged and normalized time-dependent responses of FD1 had to be larger than 0.6 (other thresholds ranging from 0.5 to 1 lead to similar results); and *2*) only windows lying within intersaccadic intervals were considered, because we focused on the neural representation of spatial information, which can only be extracted from the translational optic flow during intersaccadic intervals. Within the windows defined in this way, the overall object responses and background responses of all analyzed cells (HS, VCH, and FD1) to all different stimuli were determined by time-averaging across the windows (Fig. 3, marked in light green). Delays of the intersaccadic responses with respect to intersaccadic stimulus windows, as determined by cross-correlation with the angular velocity, ranged between 15 ms for FD1 and 22.5 ms for all other cells.

Receiver Operating Characteristic Analysis

To further specify and compare the object-induced neuronal activity on the basis of HS, VCH, and FD1 cell responses, we used the so-called receiver operating characteristic (ROC) (Greiner et al. 2000). First, we used the normalized average responses of all FD1 cells in the stimulus condition when the object is shown against a nontextured background to define a criterion for the presence of an object (Fig. 3*C1*). Only if the response was above a certain value (object-defining value of 0.2 or 0.6) was an object assumed to be present in the receptive field and moving in the preferred direction. In addition, we only analyzed the responses during intersaccadic intervals, i.e., during translational motion. The points in time within intersaccadic intervals when response values exceed the respective object-defining value served as reference (object time windows) when the ROC was being constructed. For a control analysis, we used the responses of the HS cells in an equivalent way to determine the time windows in which the object is present in the cells' receptive fields.

How well the neuronal responses indicate the presence of an object was determined under the more demanding stimulus conditions, i.e., when the object is seen against a textured background. Under these conditions, it is difficult to assess whether at a given instant in time the response is elicited by an object or by the background, because the responses of all cells are affected by both object and background motion and strongly fluctuate (Fig. 3). The ROC was constructed on the basis of the amplitude of the object-induced response difference, i.e., O-cB minus nO-cB (or O-dB minus nO-dB, respectively). We define the object as being detected correctly (correct detection) if the object-induced response difference exceeds a given threshold within an object time window. Correspondingly, a "false detection" is obtained if the same threshold is exceeded outside of object time windows. By shifting the detection threshold from the smallest response difference to the largest one by 199 incremental steps, not only the percentage of correct detections increases, but also that of false detections. Useful object detection on the basis of the neuronal response profile requires the percentage of correct detections to initially increase more than the percentage of false detections when the threshold is lowered. Otherwise, correct and false detections increase, on average, in the same way. For the different thresholds, the corresponding percentages of correct vs. false detections are plotted against each other in the ROC curve. The diagonal in the ROC curve indicates that the percentage of correct and false detections increases in the same way with decreasing threshold. The diagonal thus represents chance level. We used the area under the ROC curve to quantify object detectability. The closer the area is to 0.5, the closer it is to the diagonal and the less often the object can be detected. The closer the area is to 1.0, the better the object can be detected.

Nearness Analysis

To analyze the relationship between neural responses and the corresponding distance of the fly from the arena walls and the object, we averaged the responses of HSE cells and the corresponding nearness values. This was done during selected intersaccadic intervals for three trajectories from three different flies. Criteria to select intersaccadic intervals were as follows: *1*) because HSE is mainly sensitive to horizontal motion, the horizontal velocity component had to be at least three times larger than the vertical velocity component; *2*) the duration of the intersaccadic interval had to be longer than 10 ms; and *3*) the absolute average pitch angle during the intersaccadic interval had to be smaller than 35°. Sixty-three intersaccadic intervals fulfilled all these criteria.

The nearness, i.e., the inverse of the distance between the fly and a point somewhere in the environment, was analyzed as follows. Within the receptive field of the left or right HSE cell (Hausen 1982b; Krapp et al. 2001) we chose 210 equally spaced sample points spanning 0 to −30° in elevation and −100 to +45° or −45 to 100°, respectively, in azimuth. Spacing of sample points was 5° along either axis. The frontal equatorial direction was defined as 0°; the angular positions on the left or right side in azimuth are negative and positive, respectively. Elevations above and below the equator are denoted as positive and negative values, respectively.

We calculated the distance of the head to the background for each sample point on the basis of the flight trajectory, the head orientation of the fly, and the known geometry of the flight arena. The resulting distances were first converted to nearness (N; N = 1/distance) and then weighted by the sensitivity (S) distribution of the cell to obtain the weighted nearness (N_S). The sum of weighting factors amounts to 1.

$$\sum N_S(\Psi, \theta) = \sum \left[N(\Psi, \theta) \cdot S(\Psi, \theta) \right] \quad (1)$$

where Ψ and θ represent the position in azimuth and elevation, respectively. The sensitivity distribution of HSE was equivalent to that used in the model study by Lindemann et al. (2005) (see Fig. 6, *inset*).

Statistical Analysis

To test for significant differences between samples, we employed two-sample, one-sample, and paired-sample *t*-tests (MATLAB 7.9 ttest2 and ttest, respectively). A nonparametric trend test (Mann-Kendall test; see Mann 1945; MATLAB function ktaub provided by J. Burkey) was performed to test for significant slopes of the response vs. nearness curves (see Fig. 6).

RESULTS

We analyzed the responses of individually identifiable cells (HS, VCH, and FD1 cells) in a neural circuit of the fly's visual system, which is assumed to play a role in providing spatial information and representing objects (Egelhaaf 1985b; Kimmerle and Egelhaaf 2000a, 2000b). We asked how during flight the different cells in the circuit encode spatial information about nearby objects and extended background structures.

HS and VCH cells were recorded intracellularly. FD1 cells were recorded extracellularly, because FD1 cells have a smaller axon diameter (<5 μm; Egelhaaf 1985b) than HS and VCH cells, which makes it hard to record the cells with intracellular electrodes for a sufficiently long time. FD1 cells generate full-blown action potentials, whereas HS and VCH cells respond with pronounced graded axonal membrane potential shifts to motion. In the case of HS cells, action potentials of variable amplitude are superimposed on graded potential shifts.

Object-Induced Response Changes

In the first step of the analysis, we investigated how objects encountered during intersaccadic intervals of the flight affect the responses of FD1, HS, and VCH cells. Therefore, we designed five stimulus sequences that are based on the time-dependent optic flow experienced by a semi-free-flying fly in a cubic flight arena with a side length of 0.4 m. The optic flow sequence was replayed in its original version and in modified versions, generated by virtually changing the size and texture of the flight arena and by inserting two objects close to the flight trajectory while leaving the flight trajectory unaltered. Five visual stimulus sequences were used in the experiments: *1*) nO-cB (no object, close background) is the motion sequence experienced by the fly in the original small arena with photographs of herbage on the wall. *2*) O-cB (objects, close background) is the motion sequence that would have been experienced on the same trajectory in the small arena with two objects inserted close to the flight path (Fig. 2*A*). *3*) nO-dB (no object, distant background) and *4*) O-dB (objects, distant background) are the motion sequences from the same trajectory used in *sequences 1* and *2*, but in a large flight arena (side length 2 m). The texture on the arena walls was scaled according to the increased arena size, but the locations of the objects in *sequence 4* remained unchanged relative to the flight trajectory (Fig. 2*B*). *5*) O-nB (objects, no textured background) is the reference stimulus reconstructed from the trajectory with the objects inserted at the same location as in *sequences 2* and *4*, but with nontextured arena walls. Under this condition, displacements of the background did not lead to displacements of any contours and hence did not induce any neural responses. This stimulus was used to determine those time windows in which the cell is affected by the object (see green areas in Fig. 3).

The responses to the five stimulus sequences were recorded in seven HS cells (2 HSS, 2 HSE, and 3 HSN), three VCH cells, and five FD1 cells (Fig. 3). The time course of the responses to behaviorally generated image sequences is very complex, and interpretation of its fine structure would require further analysis. Therefore, we concentrate here on some general features of these responses, which are relevant in the context of object representation and distance encoding. HS and FD1 cells respond strongly to the reference stimulus (O-nB, Fig. 3, *A1* and *C1*). Both cell types generate large transient responses when an object moves within their receptive fields in the preferred direction. VCH cells respond with smaller fluctuation amplitudes (Fig. 3*B1*). In the small arena with textured walls, the responses of all cells fluctuate strongly (nO-cB, Fig. 3, *A2*, *B2*, and *C2*, blue curves). This result indicates that even FD1, although more sensitive to small than to large motion patterns (Egelhaaf et al. 1985b), responds strongly to prominent high-contrast textures, which are present in our "background" stimulus (for an analysis of such pattern-induced responses in other cell types, see Meyer et al. 2011; O'Carroll et al. 2011). However, in the large arena, the fluctuation amplitudes of the responses of FD1 cells are reduced dramatically. In contrast, those of HS do not change much, and those of VCH cells even increase in overall amplitude (Fig. 3, *A3*, *B3*, and *C3*, blue curves). When objects are inserted into the flight arena, both HS and FD1 cells show, although to a different extent, object-induced response increments, whereas

VCH cells do not show obvious increments (Fig. 3, *A2*, *A4*, *B2*, *B4*, *C2*, and *C4*, red curves). The increments in the FD1 responses are more pronounced than those in the HS responses, which most of the time are hardly detectable relative to the overall response fluctuations. Moreover, the increments are more obvious in the large arena, especially those of FD1 cells (Fig. 3, *A3* and *B3*, red curves).

For quantification and as a basis for our conclusions, we determined the object responses and the corresponding background responses of HS, VCH and FD1 cells within those intersaccadic time windows (Fig. 3, marked in green) in which an object in front of a homogeneous background led to responses in the particular cell (O-nB condition; details about how time windows were defined are given in MATERIALS AND METHODS). To facilitate a quantitative comparison of the performance between cell types, we normalized the intersaccadic responses in the selected time windows. For each recorded cell, the responses were divided by the corresponding mean response, time-averaged over the entire data trace obtained for the small arena without object (nO-cB condition). Not surprisingly, with this type of normalization the intersaccadic responses to objects in front of a homogeneous background (Fig. 4, O-nB condition) of FD1 cells are much larger than the corresponding HS and VCH responses. In the small arena, both HS and FD1 cells show strong background and object responses during the selected intersaccadic windows. The corresponding VCH responses are smaller. Object-induced response increments (Fig. 4, compare the markers connected by dashed lines) are significant in FD1 in both the small (paired-sample *t*-test, $P < 0.01$, $n = 5$) and large arenas (paired-sample *t*-test, $P < 0.01$, $n = 5$). For HS cells, the object-induced response increment is significant only in the large arena (paired-sample *t*-test, $P < 0.05$, $n = 7$). Object induced changes in VCH responses are less consistent and not significant, regardless of arena size, as tested separately for each of the three VCH cells across sweeps (2-sample *t*-test, 2-tailed, unknown and unequal variances, $P > 0.05$ in all cells).

The background responses of HS cells obtained in the large arena are slightly but significantly reduced relative to those obtained in the small arena (paired-sample *t*-test, $P < 0.01$, $n = 7$), whereas the responses of FD1 cells decrease dramatically (paired-sample *t*-test, $P < 0.01$, $n = 5$). Likewise, the object induced responses are significantly reduced in the large compared with the small arena in FD1 cells (paired-sample *t*-test, $P < 0.05$, $n = 5$) as well as in HS cells (paired-sample *t*-test, $P < 0.01$, $n = 7$).

The response properties of the VCH cell differ dramatically from those of both HS and FD1. Most notably, the intersaccadic responses in the selected time windows of VCH in the large arena are much stronger than those obtained in the small arena (Fig. 4), both with and without the objects being present, again tested on the basis of the sweeps recorded under the respective stimulus conditions (2-sample *t*-test, unknown and unequal variances, $P < 0.01$ in all cells).

How well the presence of an object is represented in the responses of HS, VCH or FD1 cells was quantified on the basis of ROC analysis (Fig. 5). As before, this analysis was restricted to intersaccadic intervals. Before we could construct the ROC curves, we had to define the time intervals within which an object was assumed to be within the receptive field of the cells and moving in its preferred direction (object time windows). This was done on the basis of the normalized responses obtained for FD1 under the condition with objects and a nontextured background (O-nB) by setting an object-defining value, quite arbitrarily, to either 0.2 or 0.6 (see black dashed lines in Fig. 5*B*, *left*, *inset*). Small values indicate that an object is assumed to be present even at very small neural responses, although to some extent these may be the consequence of spontaneous activity fluctuations of the neuron. Hence, the number and duration of object time windows decrease with increasing object-defining value. The detectability of objects is then determined for every single cell on the basis of the area under the corresponding ROC curves for the more complex situation when the background is also textured and thus contributes to the time-dependent responses of HS, VCH, and FD1 cells. As a consequence of the pronounced response fluctuations that are affected by both the object and the background (e.g., Fig. 3), it is difficult to assess under these conditions whether at a given instant in time the response is elicited by an object or by the background. We define the object as being detected correctly (correct detection) if the difference between the responses with and without the objects (O-cB minus nO-cB for the small arena and O-dB minus nO-dB for the large arena) exceeds a given threshold within an object time window. A false detection is obtained if the same detection threshold is exceeded outside the object time windows. By shifting the detection threshold from the largest response level to smaller levels, not only the percentage of correct detections increases, but also that of false detections. The ROC curve is then obtained by plotting for the different detection thresholds the corresponding percentages of correct vs. false detections. Data points in the ROC curves above the diagonal indicate correct detections above chance level (for further details, see MATERIALS AND METHODS). We used the object-induced differences in response amplitudes instead of the responses themselves to construct ROC curves, although only the latter is present as a neural signal in the fly's brain. However, our procedure minimizes random deviations of ROC curves from the diagonal. Such deviations are present when using the responses themselves, because flight trajectories that could be used for the analysis last for only few seconds, leading to random deviations from the average response within object time windows. Apart from such random deviations, qualitatively the same conclusions were drawn from ROC analysis when the responses were used instead of the difference signals.

Figure 5*A* shows ROC curves of a single example of each cell type for an object-defining value of 0.6. The correct detection rate was plotted against the false detection rate of the objects in the small and large arenas (Fig. 5*A*, thin and thick curves). These examples suggest that the responses of HSN and FD1 indicate the presence of an object. For FD1, object detection appears to be enhanced in the large arena. In contrast, the responses of VCH do not indicate an object consistently, although the sample ROC curve of VCH obtained for the distant background is slightly below the bisecting line (Fig. 5*A*, *middle*); this deviation from chance level appears to be not systematic (see Fig. 5*B*).

The ROC analysis for the two object-defining values of 0.2 and 0.6 were quantified for each cell by calculating the areas under the ROC curves (Fig. 5*B*). These areas are significantly different from chance level (0.5, dotted lines in Fig. 5*B*) in FD1 (1-sample *t*-test, $P < 0.05$, $n = 5$) and in HS cells (1-sample

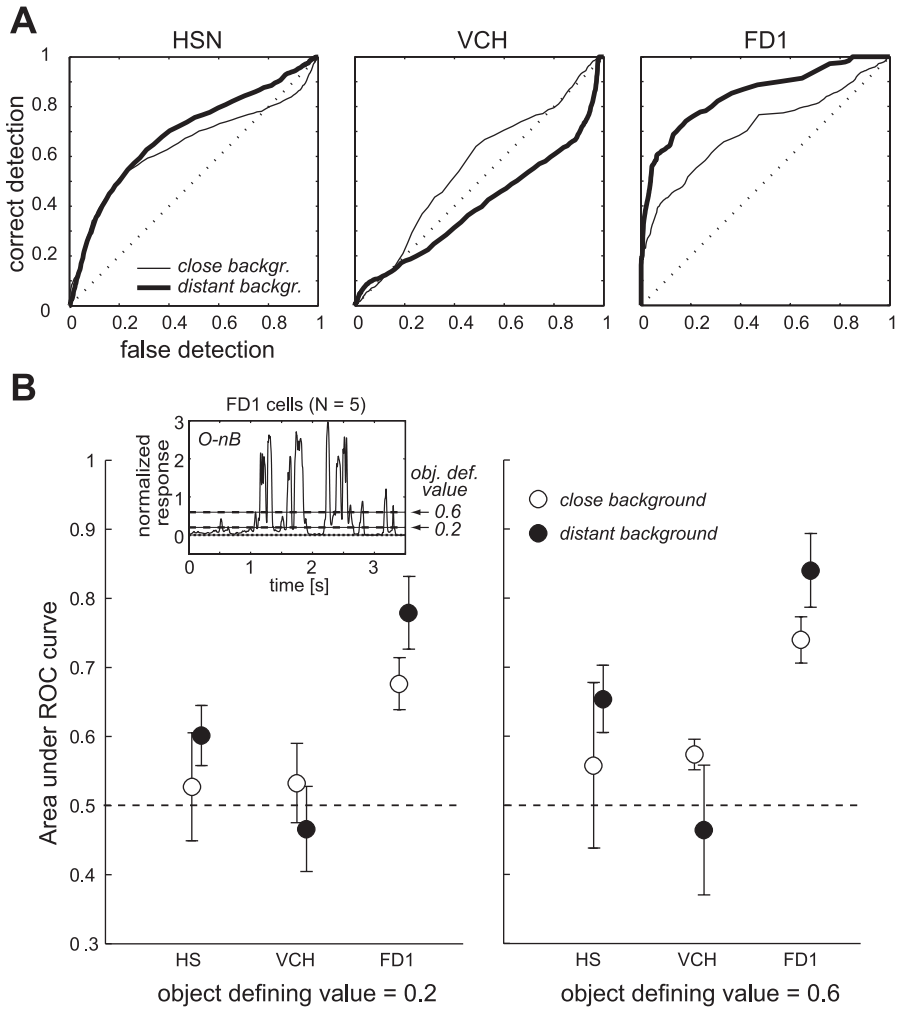

Fig. 5. *A*: example receiver operating characteristics (ROC) curves for HSN, VCH, and FD1 cells. Analysis is based on the difference between responses recorded for conditions with and without objects in the small (thin line) and large arena (thick line) . The object-defining value was set to 0.6. The dotted diagonal line indicates chance level with respect to object detection. *B*: average (±SD) area under ROC curves across cells for 2 object-defining values (0.2 and 0.6). Analysis is based on the difference between responses recorded for conditions with and without objects present in the small (open circles) and large arena (filled circles). *Inset* as shows normalized responses of FD1 to the "object-only" stimulus (O-nB), with object-defining values marked by black horizontal dashed lines. Only time windows that lay inside intersaccadic intervals were included in the ROC analysis. The larger the area below the ROC curve, the better is the detectability of the object.

t-test, $P < 0.05$, $n = 7$). Object detectability was better in the large arena than in the small arena for FD1 cells (paired-sample *t*-test, $P < 0.05$, $n = 5$) and HS cells (paired-sample *t*-test, $P < 0.05$, $n = 7$) independent of the object-defining value (Fig. 5*B*). Moreover, the area under the ROC curves was larger for FD1 ($n = 5$) than for HS ($n = 7$) cells (2-sample *t*-test, unknown and unequal variances, always $P < 0.01$) under all experimental conditions and independent of the object-defining value.

In a control analysis we employed the responses of the different HS cells to define the object time windows. On this basis we obtained qualitatively the same results as for object time windows based on FD1 responses. In particular, object detectability was much better for FD1 cells than for all three analyzed HS cells (areas under the ROC curves; close background: object-defining value of 0.2 based on HSS responses: FD1 0.75 ± 0.04, HS 0.60 ± 0.114, VCH 0.52 ± 0.06; object-defining value of 0.2 based on HSE responses: FD1 0.69 ± 0.06, HS 0.55 ± 0.08, VCH 0.55 ± 0.05; object-defining value of 0.2 based on HSN responses: FD1 0.62 ± 0.04, HS 0.51 ± 0.08, VCH 0.53 ± 0.03; object-defining value of 0.6 based on HSS responses: FD1 0.85 ± 0.05, HS 0.59 ± 0.16, VCH 0.52 ± 0.08; object-defining value of 0.6 based on HSE responses: FD1 0.78 ± 0.06, HS 0.57 ± 0.14, VCH 0.54 ± 0.04; object-defining value 0.6 based on HSN responses: FD1 0.76 ± 0.04, HS 0.54 ± 0.13, VCH 0.50 ± 0.04; distant background: object-defining value 0.2 based on HSS responses: FD1 0.08 ± 0.04, HS 66 ± 0.13, VCH 0.36 ± 0.10; object-defining value 0.2 based on HSE responses: FD1 0.75 ± 0.026, HS 0.62 ± 0.05, VCH 0.47 ± 0.08; object-defining value 0.2 based on HSN responses: FD1 0.69 ± 0.03, HS 0.58 ± 0.05, VCH 0.41 ± 0.06; object-defining value 0.6 based on HSS responses: FD1 0.96 ± 0.02, HS 0.73 ± 0.14, VCH 0.35 ± 0.13; object-defining value 0.6 based on HSE responses: FD1 0.91 ± 0.018, HS 0.69 ± 0.10, VC: 0.42 ± 0.10; object-defining value 0.6 based on HSN responses: FD1 0.91 ± 0.03, HS 0.68 ± 0.09, VCH 0.38 ± 0.11). This similarity of the ROC curves irrespective of the cell used to define the object time windows is not surprising, because the time courses of the responses of FD1 and HS cells are very similar under the O-nB condition (Fig. 3, *A1* and *C1*).

Encoding of Distances of Spatially Extended Structures in the Environment

So far, we have analyzed how objects close to the flight path of blowflies lead to response increments in different types of motion-sensitive key elements of the visual system. However, the spatial layout of the environment affects the intersaccadic depolarizations even without objects (compare responses in Fig. 4 for conditions nO-cB and nO-dB), corroborating previous findings based on a coherence analysis (Karmeier et al. 2006; Kern et al. 2005). Therefore, we systematically analyzed in the next step how spatial information is represented in the

responses of one of the HS cells, the HSE cell. We selected the HSE cell for this analysis because it is more responsive to extended patterns than the FD1 cell. We employed recordings obtained from three flight trajectories of three different flies (for details of the procedures, see MATERIALS AND METHODS). Optic flow sequences were determined for the original flight arena and five virtually enlarged ones. Because it was not necessary to restrict our analysis to intersaccadic intervals in which an object is present, we could take all intersaccadic intervals into account that had a sufficient length, were characterized by mainly forward flight, and in which head orientation was mostly horizontal. The intersaccadic responses were related to the nearness of the fly to the respective arena walls, weighted by the cell's spatial sensitivity distribution (Fig. 6*B*, *inset*).

The mean intersaccadic responses to the behaviorally generated optic flow as determined for the different-sized arenas increased (Mann-Kendall test, $P < 0.02$) with increasing overall nearness of the eye to the arena walls (Fig. 6*A*). This finding is in accordance with the results depicted in Fig. 4. Only when the arenas are relatively small, i.e., the overall nearness is large, does the mean intersaccadic response amplitude appear to saturate at a maximum response level (compare the 2 rightmost data points in Fig. 6*A*). From these results we conclude that HSE responses provide information about the distance to extended structures in the environment during translational motion during the intersaccadic interval, at least when the nearness varies on a relatively large scale.

During individual flights within a given flight arena, the nearness between the blowfly's eye and the arena wall changes only on a much finer scale. To assess whether the intersaccadic responses are also affected by the nearness on this scale, we determined the average nearness for each of the selected intersaccadic intervals as obtained from three flights in the original flight arena with 0.4-m side length. This provided us with sufficient data to allow classifying them into 6 nearness classes, each containing 21 data points (note that each intersaccadic interval contributes twice to the data set because nearness and response are different for left and right HSE). In the original flight arena, the nearness and, thus, the intersaccadic retinal velocities changed considerably during individual flights (see *x*-axis in Fig. 6*B*). The corresponding intersaccadic responses systematically increased with increasing nearness (Mann-Kendall test, $P < 0.01$). On average, the increment was almost 70% of the base value, although the standard deviations of the responses were large. However, the response increments with increasing nearness may even completely vanish when the eye of the fly comes too close to the arena walls. The large variability of the responses is likely to be a consequence of the fact that HS responses depend not only on retinal velocity (which for a given flight speed depends on the nearness) but also on the direction of motion, as well as the contrast and texture of the stimulus pattern (Egelhaaf and Borst 1989; Hausen 1982b).

DISCUSSION

Motion-sensitive cells within a small neural circuit involved in processing object information were tested with optic flow as experienced by blowflies during flights in a three-dimensional environment. By using different modifications of this behaviorally generated optic flow, we could show that during intersaccadic intervals, all three analyzed cell types respond not only to nearby objects but also to changes in the distance to the background structures, although to a different extent. Whereas HS cells and, in particular, FD1 cells show significant object-induced response increments even in front of a textured background, VCH cells reveal obvious object responses only if there is no background texture. The intersaccadic background responses of HS and FD1 cells decrease with increasing distance to the animal; the decrease is much stronger in FD1 than in HS cells. This strong dependence of FD1 on background distance is concluded to be the consequence of the activity of VCH, which with increasing distance dramatically increases its activity and, thus, its inhibitory strength.

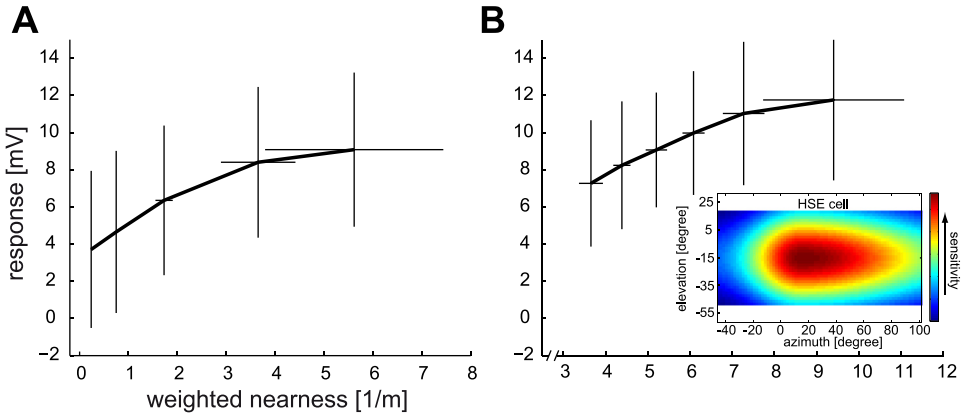

Fig. 6. *A*: average responses (±SD) of 2 left and 2 right HSE cells during 63 intersaccadic intervals selected from 3 flight trajectories are plotted against the corresponding average weighted nearness (±SD) in virtual cubic arenas of 5 different sizes [edge lengths: 0.41, 0.55, 1.05, 2.35, and 7.35 m; minimum (maximum) number of sweeps per cell, trajectory, and arena size: 1 (3), median: 2; total number of sweeps: 119]. *B*: averaged intersaccadic responses (±SD) of 5 left and 5 right HSE are plotted against the average weighted nearness during 63 individual intersaccadic intervals selected from 3 flight trajectories in the original flight arena with edge length of 0.4 m. The responses were sorted by increasing nearness and then attributed to 6 groups with 21 data points per group. The vertical and horizontal lines show the SDs of responses and nearness, respectively, across the data values within 1 group [minimum (maximum) number of sweeps per cell and trajectory: 1 (7), median: 3; total number of sweeps: 100]. *Inset*: the modeled local sensitivity distribution of the right HSE cell. The contours are plotted in cylindrical projection. Red areas indicate higher sensitivities (see color bar at *right*). For determining the nearness values, the area under the sensitivity distribution was set at 1. The frontal equatorial viewing direction is at 0° azimuth and elevation. The most sensitive position in elevation for HSE is at −15°. The sensitivity values sum up to 1.

Object and Background Segregation

The FD1 cell has been shown to respond to the motion of objects, when presented either alone or in front of a background moving at a different velocity (Egelhaaf 1985b, 1985c; Kimmerle and Egelhaaf 2000a, 2000b). The functional properties of the FD1 cell differ markedly with respect to its size tuning from those of several other types of object-sensitive neurons in insects (review: Nordström 2012). In both dragonflies and hoverflies, but also in male blowflies, neurons have been characterized that are extremely specific for very small targets. These cells are assumed to play an important role, depending on the species under consideration, in detecting and catching prey insects, in the social encounter between conspecifics, or in mating behavior (Nordström and O'Carroll 2006; Nordström et al. 2006; Trischler et al. 2007). The preferred object size of FD1 is much larger than that of these small-target neurons, hinting at a very different function. Accordingly, FD1 cells have been proposed to be involved in detecting stationary objects in cluttered environments that may be obstacles for the moving animal or that may serve as landing sites or landmarks for navigation (Egelhaaf 1985b; Kimmerle and Egelhaaf 2000a, 2000b).

Although HS cells are most sensitive to spatially extended patterns and are thought to be major output cells of the neuronal network underlying optomotor course control (Hausen 1981; Hausen and Wehrhahn 1983; Wehrhahn 1985), they also provide spatial information during the intersaccadic interval (Karmeier et al. 2006; Kern et al. 2005). Accordingly, they are also responsive to objects. Moreover, their responses to objects as well as to other stimulus discontinuities are even enhanced by motion adaptation (Kurtz et al. 2010; Liang et al. 2008, 2011; Maddess and Laughlin 1985). These findings suggest that HS cell may play a role, probably in concert with other neurons such as FD1, in mediating object-related behavior.

Possible Mechanisms Underlying Object Specificity

Object sensitivity of FD1 cells is based on inhibition during large-field background motion (Egelhaaf 1985b, 1985c; Egelhaaf and Borst 1993). As an inhibitory element, the GABAergic VCH cell could be identified (Warzecha et al. 1993). This cell is supposed to inhibit the FD1 cell via distributed dendritic synapses, most likely operating on the local retinotopic input elements of FD1 (Gauck et al. 1997; Hennig et al. 2008). The VCH cell receives its ipsilateral input from HS cells via dendrodendritic electrical synapses, its contralateral excitatory input from H1 and H2 cells, and inhibitory input from the Hu cell (see Fig. 1). As a consequence of input from HS cells via dendrodendritic electrical synapses, VCH cell dendrites serve as a kind of low-pass filter, which produces a spatial blur of the so-called motion image in the dendritic activity profile (Cuntz et al. 2003; Hennig et al. 2008). This property might well be functionally relevant in the context of object detection, because small motion patterns might be more affected by spatial low-pass filtering than larger motion patterns. In this way, inhibition of FD1 via VCH could be more pronounced for large than for small patterns (Hennig et al. 2008).

At first sight, the strong intersaccadic responses of VCH in the large flight arena are surprising, because the retinal image velocities decrease with increasing distance of the eye from the arena wall. The strong intersaccadic responses in the large flight arena are likely to have two reasons, both originating from the VCH cell's contralateral input. On one hand, the inhibitory input originating from the Hu cell (see Fig. 1) might be weaker in the large arena compared with the small arena, where the translational optic flow is larger, and thus might stimulate the inhibitory cell more than in the large arena. Hu can be assumed to have a relatively strong inhibitory impact on VCH during front-to-back motion, because it can counteract to a large extent the strong simultaneous excitatory input mediated via the HS cells (Egelhaaf et al. 1993). On the other hand, the H1 cell shows a much larger intersaccadic activity during stimulation with behaviorally generated optic flow in the large than in the small flight arena. This characteristic most likely is a consequence of a release from inhibition in the large arena that in the small arena suppresses residual excitatory rotational input during the intersaccadic intervals (van Hateren et al. 2005).

Distance Encoding in Three-Dimensional Environments

HS cells as well as other LPTCs have been shown to encode information about translational optic flow and, thus, implicitly about the spatial relation of the animal to its environment during intersaccadic intervals (Karmeier et al. 2006; Kern et al. 2005). In this experiment we analyzed intersaccadic HSE responses to behaviorally generated optic flow by relating them to the distance between the eye and the background walls in a three-dimensional environment (Fig. 6). We found that the responses of the analyzed HSE cells generally increase with the nearness of extended structures in the environment. This conclusion holds not only if the arena is virtually enlarged, leading to relatively large nearness differences between the different arenas, but also during individual flights within a given arena, where the nearness varies only relatively little between the intersaccadic intervals. The large standard deviations of the intersaccadic response underline the well-known fact that responses of fly LPTCs depend not only on pattern velocity but also on the direction of local and global motion as well as on stimulus parameters such as the texture of the environment and its contrast (Borst and Haag 2002; Egelhaaf 2006, 2009; Hausen 1981, 1984). Most of these parameters vary within free flights in our flight arena and thus might have affected the neural responses.

Functional Considerations

It is not easy to infer the functional significance of a visual neuron from its response properties alone, especially if the stimuli used in the experiments deviate much from the spatio-temporal conditions that are encountered by the animal under its normal behavioral operating conditions. Therefore, we employed behaviorally generated optic flow for stimulation. These stimuli come as close as is currently possible to what the fly has seen during free-flight maneuvers. The optic flow can be segregated into mainly rotational segments, which are shaped by short, rapid saccadic turns of the animal, and segments of basically straight flight that are dominated by translational image motion, at least if the distance from the fly to objects in the environment is not too large. LPTCs, such as HS or FD1 cells, may show large responses during the intersaccadic intervals. On the basis of an analysis of these responses, we concluded in the present study, in accordance with

previous results (Karmeier et al. 2006; Kern et al. 2005; van Hateren et al. 2005), that these cells may play prominent roles in representing information about translational motion and, thus, indirectly about the spatial layout of the environment. A functional role of HS and FD1 cells in representing translational motion and, thus, object and distance information is also suggested by the fact that the translational optic flow during intersaccadic intervals usually covers a velocity range that is represented by monotonically increasing neural responses. In contrast, a monotonic dependence is not present during the most prominent rotations of the animal, i.e., during saccadic turns, with their retinal velocities of up to 3,000°/s. During saccades with peak velocities of 500°/s and above, the motion detection system operates beyond its optimal operating range for most of the time. Accordingly, saccades leading to movements in the HS cell's preferred direction do not induce larger responses than the much smaller translational velocities during the intersaccadic interval, if the fly is close to environmental structures (Karmeier et al. 2006; Kern et al. 2005).

In recent studies it became evident that the response properties of fly LPTCs are affected by the behavioral state of the animal. Most prominently, the response amplitudes of LPTCs increase if the animal is behaviorally active during the electrophysiological recording, such as beating its halteres (the gyroscopic sensors evolved from the fly's hindwings), flying on a tether, or walking on a treadmill (Chiappe et al. 2010; Maimon et al. 2010; Rosner et al. 2010). Moreover, there is evidence that the dynamic range of velocity tuning is somewhat shifted toward larger velocities during behavioral activity (Chiappe et al. 2010; Jung et al. 2011). Because it is currently not possible to monitor the responses of LPTCs during free flight, we replayed in our electrophysiological experiments on tethered animals the optic flow experienced during free flight. Are our conclusions affected by this limitation? Although this question cannot yet be answered definitely, we are confident that the described changes in LPTC properties, such as the general increase in response amplitude, during behavioral activity would not alter our basic conclusion. Moreover, if a shift in the velocity tuning toward higher velocities were also effective during stimulation with behaviorally generated optic flow, it would mainly affect the responses during flight maneuvers that lead to high retinal velocities. For intersaccadic intervals, which were considered in this study, high velocities are present close to objects or arena walls. A shift in velocity tuning toward higher velocities would ameliorate the saturation in the dependency of the response on nearness and thus would even improve the encoding of distance information. Such a change would strengthen our conclusion that LPTCs may encode spatial information during intersaccadic intervals.

GRANTS

This study was supported by the Deutsche Forschungsgemeinschaft.

DISCLOSURES

No conflicts of interest, financial or otherwise, are declared by the authors.

AUTHOR CONTRIBUTIONS

Author contributions: P.L., R. Kern, R. Kurtz, and M.E. conception and design of research; P.L., J.H., and R. Kern performed experiments; P.L., J.H., and R. Kern analyzed data; P.L., J.H., R. Kern, R. Kurtz, and M.E. interpreted results of experiments; P.L. and R. Kurtz prepared figures; P.L. and M.E. drafted manuscript; P.L., J.H., R. Kern, R. Kurtz, and M.E. approved final version of manuscript; R. Kern, R. Kurtz, and M.E. edited and revised manuscript.

REFERENCES

Boeddeker NL, Dittmar L, Stürzl W, Egelhaaf M. The fine structure of honeybee head and body yaw movements in a homing task. *Proc Biol Sci* 277: 1899–1906, 2010.

Boeddeker N, Lindemann JP, Egelhaaf M, Zeil J. Responses of blowfly motion-sensitive neurons to reconstructed optic flow along outdoor flight paths. *J Comp Physiol A Neuroethol Sens Neural Behav Physiol* 191: 1143–1155, 2005.

Borst A, Haag J. Neural networks in the cockpit of the fly. *J Comp Physiol A Neuroethol Sens Neural Behav Physiol* 188: 419–437, 2002.

Borst A, Haag J, Reiff DF. Fly motion vision. *Annu Rev Neurosci* 33: 49–70, 2010.

Braun E, Dittmar L, Boeddeker N, Egelhaaf M. Prototypical components of honeybee homing flight behavior depend on the visual appearance of objects surrounding the goal. *Front Behav Neurosci* 6: 1, 2012.

Braun E, Geurten B, Egelhaaf M. Identifying prototypical components in behaviour using clustering algorithms. *PLoS One* 5: e9361, 2010.

Chiappe ME, Seelig JD, Reiser MB, Jayaraman V. Walking modulates speed sensitivity in *Drosophila* motion vision. *Curr Biol* 20: 1470–1475, 2010.

Cuntz H, Haag J, Borst A. Neural image processing by dendritic networks. *Proc Natl Acad Sci USA* 100: 11082–11085, 2003.

Dahmen HJ, Franz MO, Krapp HG. Extracting ego-motion from optic flow: limits of accuracy, and neuronal filters. In: *Computational, Neural and Ecological Constraints of Visual Motion Processing*, edited by Zanker JM, Zeil J. Berlin: Springer, 2000.

Dürr V, Egelhaaf M. In vivo calcium accumulation in presynaptic and postsynaptic dendrites of visual interneurons. *J Neurophysiol* 82: 3327–3338, 1999.

Eckert H, Dvorak DR. The centrifugal horizontal cells in the lobula plate of the blowfly, *Phaenicia sericata*. *J Insect Physiol* 29: 547–560, 1983.

Eckmeier D, Geurten BR, Kress D, Mertes M, Kern R, Egelhaaf M, Bischof HJ. Gaze strategy in the free flying zebra finch (*Taeniopygia guttata*). *PLoS One* 3: e3956, 2008.

Egelhaaf M. On the neuronal basis of figure-ground discrimination by relative motion in the visual system of the fly. I. Behavioural constraints imposed on the neuronal network and the role of the optomotor system. *Biol Cybern* 52: 123–140, 1985a.

Egelhaaf M. On the neuronal basis of figure-ground discrimination by relative motion in the visual system of the fly. II. Figure-detection cells, a new class of visual interneurones. *Biol Cybern* 52: 195–209, 1985b.

Egelhaaf M. On the neuronal basis of figure-ground discrimination by relative motion in the visual system of the fly. III. Possible input circuitries and behavioural significance of the FD cells. *Biol Cybern* 52: 267–280, 1985c.

Egelhaaf M. The neural computation of visual information. In: *Invertebrate Vision,* edited by Warrant E, Nielsson DE. Cambridge, UK: Cambridge University Press, 2006.

Egelhaaf M. Insect motion vision. *Scholarpedia* 4: 1671, 2009.

Egelhaaf M, Borst A. Transient and steady-state response properties of movement detectors. *J Opt Soc Am A* 6: 116–127, 1989.

Egelhaaf M, Borst A. Movement detection in arthropods. In: *Visual Motion and its Role in the Stabilization of Gaze*, edited by Wallman J, Miles FA. Amsterdam: Elsevier, 1993, p. 53–77.

Egelhaaf M, Borst A, Warzecha AK, Flecks S, Wildemann A. Neural circuit tuning fly visual interneurons to motion of small objects. II. Input organization of inhibitory circuit elements by electrophysiological and optical recording techniques. *J Neurophysiol* 69: 340–351, 1993.

Egelhaaf M, Kern R, Krapp HG, Kretzberg J, Kurtz R, Warzecha AK. Neural encoding of behaviourally relevant visual-motion information in the fly. *Trends Neurosci* 25: 96–102, 2002.

Frost BJ, Nakayama K. Single visual neurons code opposing motion independent of direction. *Science* 220: 744–745, 1983.

Gauck V, Egelhaaf M, Borst A. Synapse distribution on VCH, an inhibitory, motion-sensitive interneuron in the fly visual system. *J Comp Neurol* 381: 489–499, 1997.

Geurten B, Kern R, Braun E, Egelhaaf M. A syntax of hoverfly flight prototypes. *J Exp Biol* 213: 2461–2475, 2010.

Greiner M, Pfeiffer D, Smith RD. Principles and practical application of the receiver-operating characteristic analysis for diagnostic tests. *Prev Vet Med* 45: 23–41, 2000.

Haag J, Borst A. Recurrent network interactions underlying flowfield selectivity of visual interneurons. *J Neurosci* 21: 5685–5692, 2001.

Haag J, Borst A. Dendro-dendritic interactions between motion-sensitive large-field neurons in the fly. *J Neurosci* 22: 3227–3233, 2002.

Hausen K. Functional characterization and anatomical identification of motion sensitive neurons in the lobula plate of the blowfly *Calliphora erythrocephala*. *Z Naturforsch* 31: 629–633, 1976.

Hausen K. Monocular and binocular computation of motion in the lobula plate of the fly. *Verh Dt Zool Ges* 74: 49–70, 1981.

Hausen K. Motion sensitive interneurons in the optomotor system of the fly. I. The horizontal cells: structure and signals. *Biol Cybern* 45: 143–156, 1982a.

Hausen K. Motion sensitive interneurons in the optomotor system of the fly. II. The horizontal cells: receptive field organization and response characteristics. *Biol Cybern* 46: 67–79, 1982b.

Hausen K. The lobula-complex of the fly: structure, function and significance in visual behaviour. In: *Photoreception and Vision in Invertebrates*, edited by Ali MA. New York: Plenum, 1984, p. 523–559.

Hausen K, Wehrhahn C. Microsurgical lesion of horizontal cells changes optomotor yaw responses in the blowfly *Calliphora erythrocephala*. *Proc R Soc Lond B Biol Sci* 219: 211–216, 1983.

Hennig P, Möller R, Egelhaaf M. Distributed dendritic processing facilitates object detection: a computational analysis on the visual system of the fly. *PLoS One* 3: e3092, 2008.

Hennig P, Kern R, Egelhaaf M. Binocular integration of visual information: a model study on naturalistic optic flow processing. *Front Neural Circuits* 5: 4, 2011.

Horstmann W, Egelhaaf M, Warzecha AK. Synaptic interactions increase optic flow specificity. *Eur J Neurosci* 12: 2157–2165, 2000.

Jung SN, Borst A, Haag J. Flight activity alters velocity tuning of fly motion-sensitive neurons. *J Neurosci* 31: 9231–9237, 2011.

Karmeier K, van Hateren JH, Kern R, Egelhaaf M. Encoding of naturalistic optic flow by a population of blowfly motion-sensitive neurons. *J Neurophysiol* 96: 1602–1614, 2006.

Kern R, van Hateren JH, Egelhaaf M. Representation of behaviourally relevant information by blowfly motion-sensitive visual interneurons requires precise compensatory head movements. *J Exp Biol* 209: 1251–1260, 2006.

Kern R, van Hateren JH, Michaelis C, Lindemann JP, Egelhaaf M. Function of a fly motion-sensitive neuron matches eye movements during free flight. *PLoS Biol* 3: e171, 2005.

Kimmerle B, Egelhaaf M, Srinivasan MV. Object detection by relative motion in freely flying flies. *Naturwissenschaften* 83: 380–381, 1996.

Kimmerle B, Egelhaaf M. Detection of object motion by a fly neuron during simulated translatory flight. *J Comp Physiol A* 186: 21–31, 2000b.

Kimmerle B, Egelhaaf M. Performance of fly visual interneurons during object fixation. *J Neurosci* 20: 6256–6266, 2000a.

Koenderink JJ. Optic Flow. *Vision Res* 26: 161–180, 1986.

Kral K. Behavioural-analytical studies of the role of head movements in depth perception in insects, birds and mammals. *Behav Processes* 64: 1–12, 2003.

Kral K. Comparison of the use of active vision for depth perception in three grasshopper families (Orthoptera: Caelifera). *Ann Entomol Soc Am* 102: 339–345, 2009.

Krapp HG, Hengstenberg R, Egelhaaf M. Binocular contribution to optic flow processing in the fly visual system. *J Neurophysiol* 85: 724–734, 2001.

Kurtz R, Dürr V, Egelhaaf M. Dendritic calcium accumulation associated with direction selective adaptation in visual motion sensitive neurons in vivo. *J Neurophysiol* 84: 1914–1923, 2000.

Kurtz R, Egelhaaf M, Meyer HG, Kern R. Adaptation accentuates responses of fly motion-sensitive visual neurons to sudden stimulus changes. *Proc R Soc Lond B Biol Sci* 276: 3711–3719, 2009.

Lappe M, Bremmer F, van den Berg AV. Perception of self-motion visual flow. *Trends Cogn Sci* 3: 329–336, 1999.

Liang P, Kern R, Egelhaaf M. Motion adaptation enhances object-induced neural activity in three-dimensional virtual environment. *J Neurosci* 28: 11328–11332, 2008.

Liang P, Kern R, Kurtz R, Egelhaaf M. Impact of visual motion adaptation on neural responses to objects and its dependence on the temporal characteristics of optic flow. *J Neurophysiol* 105: 1825–1834, 2011.

Lindemann JP, Kern R, Michaelis C, Meyer P, van Hateren JH, Egelhaaf M. FliMax, a novel stimulus device for panoramic and high-speed presentation of behaviourally generated optic flow. *Vision Res* 43: 779–791, 2003.

Lindemann JP, Kern R, van Hateren JH, Ritter H, Egelhaaf M. On the computations analysing natural optic flow: quantitative model analysis of the blowfly motion vision pathway. *J Neurosci* 25: 6435–6448, 2005.

Logan DJ, Duffy CJ. Cortical area MSTd combines visual cues to represent 3-D self-movement. *Cereb Cortex* 16: 1494–1507, 2006.

Longuet-Higgins HC, Prazdny K. The interpretation of a moving retinal image. *Proc R Soc Lond B Biol Sci* 208: 385–397, 1980.

Maddess T, Laughlin SB. Adaptation of the motion-sensitive neuron H1 is generated locally and governed by contrast frequency. *Proc R Soc London B Biol Sci* 225: 251–275, 1985.

Maimon G, Straw AD, Dickinson MH. Active flight increases the gain of visual motion processing in *Drosophila*. *Nat Neurosci* 13: 393–399, 2010.

Mann HB. Nonparametric tests against trends. *Econometrica* 13: 245–259, 1945.

Meyer GH, Lindemann JP, Egelhaaf M. Pattern-dependent response modulations in motion-sensitive visual interneurons - a model study. *PLoS One* 6: e21488, 2011.

Miles FA. The neural processing of 3-D visual information: evidence from eye movements. *Eur J Neurosci* 10: 811–822, 1998.

Nordström K. Neural specializations for small target detection in insects. *Curr Opin Neurobiol*. In press.

Nordström K, Barnett PD, O'Carroll DC. Insect detection of small targets moving in visual clutter. *PLoS Biol* 4: e54, 2006.

Nordström K, O'Carroll DC. Small object detection neurons in female hoverflies. *Proc Biol Sci* 273: 1211–1216, 2006.

O'Carroll DC, Barnett PD, Nordström K. Local and global responses of insect motion detectors to the spatial structure of natural scenes. *J Vis* 11: 20, 2011.

Prazdny K. Ego-motion and relative depth map from optical-flow. *Biol Cybern* 36: 87–102, 1980.

Regan D, Beverley KI. Figure-ground segregation by motion contrast and by luminance contrast. *J Opt Soc Am A* 1: 433–442, 1984.

Reichardt W, Poggio T, Hausen K. Figure-ground discrimination by relative movement in the visual system of the fly. Part II: Towards the neuronal circuitry. *Biol Cybern* 46: 1–30, 1983.

Rosner R, Egelhaaf M, Warzecha AK. Behavioural state affects motion-sensitive neurones in the fly visual system. *J Exp Biol* 213: 331–338, 2010.

Schilstra C, van Hateren JH. Blowfly flight and optic flow. I. Thorax kinematics and flight dynamics. *J Exp Biol* 202: 1481–1490, 1999.

Srinivasan MV, Lehrer M, Horridge GA. Visual figure-ground discrimination in the honeybee: the role of motion parallax at boundaries. *Proc R Soc Lond B Biol Sci* 238: 331–350, 1990.

Trischler C, Boeddeker N, Egelhaaf M. Characterisation of a blowfly male-specific neuron using behaviourally generated visual stimuli. *J Comp Physiol A* 193: 559–572, 2007.

van Hateren JH, Kern R, Schwerdtfeger G, Egelhaaf M. Function and coding in the blowfly H1 neuron during naturalistic optic flow. *J Neurosci* 25: 4343–4352, 2005.

van Hateren JH, Schilstra C. Blowfly flight and optic flow. II. Head movements during flight. *J Exp Biol* 202: 1491–1500, 1999.

Virsik RP, Reichardt W. Detection and tracking of moving objects by the fly *Musca domestica*. *Biol Cybern* 23: 83–98, 1976.

Warren WH, Kay JR, Zosh BA, Duchon WD, Sahuc AP. Optic flow is used to control human walking. *Nat Neurosci* 4: 213–216, 2001.

Warzecha AK, Egelhaaf M, Borst A. Neural circuit tuning fly visual interneurons to motion of small objects. I. Dissection of the circuit by pharmacological and photoinactivation techniques. *J Neurophysiol* 69: 329–339, 1993.

Wehrhahn C. Visual guidance of flies during flight. In: *Comprehensive Insect Physiology, Biochemistry and Pharmacology. Nervous Systems: Sensory*, edited by Kerkut GA, Gilbert LI. Oxford, UK: Pergamon, 1985, vol. 6, p. 673–684.

Wylie DR, Forst BJ. Responses of neurons in the nucleus of the basal optic root to translational and rotational flowfields. *J Neurophysiol* 81: 267–276, 1999.